

# **Label-free and noninvasive optical detection of the distribution of nanometer-size mitochondria in single cells**

Xuantao Su  
Yuanyuan Qiu  
Leah Marquez-Curtis  
Manisha Gupta  
Clarence E. Capjack  
Wojciech Rozmus  
Anna Janowska-Wieczorek  
Ying Y. Tsui

# Label-free and noninvasive optical detection of the distribution of nanometer-size mitochondria in single cells

Xuantao Su,<sup>a,b,\*</sup> Yuanyuan Qiu,<sup>c,\*</sup> Leah Marquez-Curtis,<sup>c</sup> Manisha Gupta,<sup>b</sup> Clarence E. Capjack,<sup>b</sup> Wojciech Rozmus,<sup>d</sup> Anna Janowska-Wieczorek,<sup>c,e</sup> and Ying Y. Tsui<sup>b</sup>

<sup>a</sup>Shandong University, School of Control Science & Engineering, Department of Biomedical Engineering, Jinan, China 250061

<sup>b</sup>University of Alberta, Department of Electrical and Computer Engineering, Edmonton, Alberta, T6G 2V4 Canada

<sup>c</sup>Canadian Blood Services, Edmonton, Alberta, T6G 2R8 Canada

<sup>d</sup>University of Alberta, Department of Physics, Edmonton, Alberta, T6G 2G7 Canada

<sup>e</sup>University of Alberta, Department of Medicine, Edmonton, Alberta, T6G 2V2 Canada

**Abstract.** A microfluidic flow cytometric technique capable of obtaining information on nanometer-sized organelles in single cells in a label-free, noninvasive optical manner was developed. Experimental two-dimensional (2D) light scattering patterns from malignant lymphoid cells (Jurkat cell line) and normal hematopoietic stem cells (cord blood CD34+ cells) were compared with those obtained from finite-difference time-domain simulations. In the simulations, we assumed that the mitochondria were randomly distributed throughout a Jurkat cell, and aggregated in a CD34+ cell. Comparison of the experimental and simulated light scattering patterns led us to conclude that distinction from these two types of cells may be due to different mitochondrial distributions. This observation was confirmed by conventional confocal fluorescence microscopy. A method for potential cell discrimination was developed based on analysis of the 2D light scattering patterns. Potential clinical applications using mitochondria as intrinsic biological markers in single cells were discussed in terms of normal cells (CD34+ cell and lymphocytes) versus malignant cells (THP-1 and Jurkat cell lines). © 2011 Society of Photo-Optical Instrumentation Engineers (SPIE). [DOI: 10.1117/1.3583577]

Keywords: biomedical instrumentation; label-free detection; flow cytometry; microfluidics; light scattering; single cells; mitochondria; finite-difference time-domain.

Paper 10610R received Nov. 16, 2010; revised manuscript received Mar. 28, 2011; accepted for publication Apr. 7, 2011; published online Jun. 1, 2011.

## 1 Introduction

Developments in microscopy techniques have enabled the observation of organelles within cells at the nanometer scale, as well as viruses that are interacting with cells.<sup>1-4</sup> These methods for obtaining cellular information fall into two categories. First, fluorescence labeling has been used to enhance the contrast of the cell components, thus allowing otherwise transparent phase samples to be observed and even super-resolution viewing of cells at tens of nanometers by using the stochastic optical reconstruction microscopy (STORM) technique.<sup>3</sup> A second method for obtaining high resolution images involves using shorter wavelength illumination, for example, the use of transmission electron microscopy (TEM) on thinly sliced biological cell specimens.<sup>4</sup> All the above methods are invasive to the cells.

Hematopoietic stem cells have the remarkable capability to differentiate into mature blood cells of all lineages (erythroid, myeloid and lymphoid) while maintaining their ability to self-renew.<sup>5</sup> Hence they have been used to re-establish the hematopoietic function in patients with damaged or defective bone marrow or immune system.<sup>6</sup> Human hematopoi-

etic stem cells and progenitors express the surface glycoprotein CD34, a marker which allows their isolation by immunomagnetic labeling.<sup>7</sup> A label-free technique is preferred for the study of stem cells in order not to disturb their biological functions.

The light scattering method may be used as a noninvasive, label-free technique for obtaining cellular information.<sup>8-17</sup> Light scattering spectroscopy (LSS) has been used for obtaining information of submicrometer organelles noninvasively.<sup>11-14</sup> Recently, LSS has been combined with confocal microscopy, the confocal light absorption and scattering spectroscopic microscopy (CLASS), for cellular observation without exogenous labels.<sup>13,14</sup> Alternatively, our group has demonstrated the 2D light scattering intensity patterns can be analyzed to obtain submicron-scale information of the cells.<sup>15,16,18</sup> Analysis of the light scattering patterns provides very useful cellular information. As we will later show in this paper, 2D light scattering patterns may be used for cell discrimination or the recognition of various physiological states in cells of the same kind.

In Sec. 2 we will describe our fiber-coupled microfluidic cytometer for measuring 2D light scattering patterns from single cells. We have obtained experimental 2D light scattering patterns from different cells including leukemic cell lines (Jurkat and THP-1) and normal hematopoietic cells (CD34+ cells and lymphocytes). Detailed numerical simulations are performed to

\*These authors contributed equally to this paper.

Address all correspondence to: Xuantao Su, Shandong University, School of Control Science & Engineering, Department of Biomedical Engineering, Jinan, China 250061, Tel: 86-531-88399089; E-mail: xtsu@sdu.edu.cn.

examine the effect of varying the number, the size, and the distribution of mitochondria in order to aid in our understanding of these light scattering patterns. By analyzing the 2D light scattering patterns, we have established criteria that can be used to discriminate between different types of cells. We expect that these criteria may be used in the future to determine the physiological status of cells or for cell sorting.

## 2 Methods

### 2.1 A Fiber-Coupled Microfluidic Cytometer

The light scattering microfluidic cytometer has three major components: the illumination light source, the microfluidic chip, and the detector. The coupling of light into the microfluidic channel is very important and has been studied intensively. For example, a tapered microchannel has been fabricated that can couple laser light into a microfluidic channel.<sup>19</sup> Another way is to use a prism to couple a laser beam into a microfluidic channel.<sup>16</sup> In this work, we adopted the fiber coupling technique to illuminate a single scatterer within the microfluidic flow. This has three major advancements: 1., the rigorous microchannel fabrication is no longer necessary as compared with Ref. 19; 2., the coupling of the laser light to the microfluidic channel is much easier, while the tapered waveguide structure (Ref. 19) and the prism coupling technique (Ref. 16) require tedious alignment of the laser system with the microfluidic chip; and 3., with the optical fiber the chip can be moved around in the experimental area with the laser-fiber coupling system kept fixed, which is very convenient for bio-experiments.

An illustration of the experimental setup of our light scattering microfluidic cytometer is shown in Fig. 1. The laser light (532 nm, DPSS laser, Laserglow Technologies, Ontario, Canada) is coupled into one end of the fiber (105/125  $\mu\text{m}$ , Thorlabs, New Jersey) via a  $4\times$  microscope objective with a numerical aperture (NA) of 0.1. In our setup, an  $\sim 2$  mW input laser power is used. A charge coupled device (CCD) sensor (ICX204AK, Sony, Japan) is in close contact with the microfluidic chip to maximize the observation angle. The imaging system consists of a microscope objective and a CCD detector is placed on the opposite side of the microfluidic chip. The imaging sys-

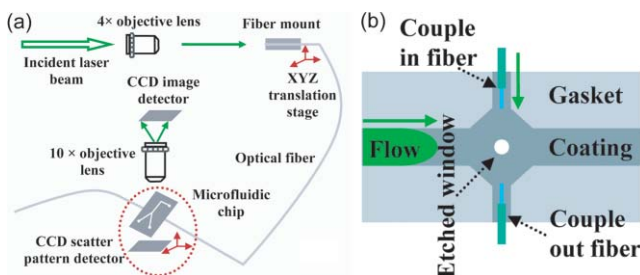


**Fig. 1** A schematic diagram for the label-free fiber-coupled microfluidic cytometer. (a) A laser beam coupled to a microfluidic chip. An immobilized single scatterer can be examined by the image system on top of the microfluidic chip, and a CCD detector underneath the microfluidic chip obtains the 2D light scattering patterns. The upper XYZ translation stage helps for coupling the laser light into the optical fiber, while the lower one is used to locate the single scatterer and to align the system. (b) Diagram of the observation window area. The fiber is perpendicular to the flow direction. The observation window is approximately  $400 \mu\text{m}$ , and the channel width is  $\sim 600 \mu\text{m}$ .

tem is used to locate a scatterer of interest. Figure 1(b) shows a detailed illustration of the sensing area of the microfluidic channel. The microfluidic channel was fabricated by sandwiching three layers: a glass slide on the top, a gasket in the middle, and a glass slide with a thin coated chrome film of  $\sim 80$  nm in the bottom. The three layers were bonded together using UV curable epoxy.<sup>16</sup> The flow in the channel was pressure-driven by using a syringe. As a cell arrived at the observation area, it was immobilized by manipulating the syringe to apply positive and negative pressures to the flow. There are two fibers: one to couple the laser light into the microfluidic channel to excite the single scatterer that has been immobilized, and the other to couple the light that is transmitted through the single scatterer out from the channel. The couple-out fiber helps to reduce the background noise that is due to scattering from the surroundings, such as that originating from the rough channel edges. A microsize observation window that is located in the center of the  $600\text{-}\mu\text{m}$  wide microfluidic channel is  $\sim 400 \mu\text{m}$  in diameter. The microsize window helps to reduce the scattering of the background light in the microfluidic channel into the CCD sensor. The optical fiber is with a NA of 0.22 and the fiber end is  $\sim 2$  mm from the center of the observation window. The laser beam from the optical fiber will be expanded to  $\sim 700\text{-}\mu\text{m}$  while arriving at the observation window area. For a  $10\text{-}\mu\text{m}$  cell excited by a  $700 \mu\text{m}$  width beam, we assume a plane wave excitation for the light scattering analysis.

### 2.2 Preparation of the Cells for the Light Scattering Measurements

The human hematopoietic cell lines Jurkat (acute T-cell leukemia) and THP-1 (acute monocytic leukemia) were obtained from the American Type Culture Collection (Rockville, Maryland) and grown in RPMI media (Invitrogen, Burlington, Ontario, Canada) supplemented with 10% bovine growth serum (BGS, Hyclone, ThermoFisher Scientific, Nepean, Ontario, Canada).

Cord blood samples were obtained from healthy full-term newborn infants (with the mothers' informed consent), all in accordance with the guidelines approved by the University of Alberta Health Research Ethics Board. Light-density mononuclear cells (MNC) were separated by centrifugation using a 60% Percoll density gradient (1.077 g/mL, Amersham, Uppsala, Sweden). CD34+ cells were isolated from the light-density MNC interphase using the Miltenyi MACS system (Miltenyi Biotech, Auburn, California) as described previously.<sup>20</sup> Lymphocytes were obtained from whole blood after density gradient centrifugation using Lymphocyte-poly (1.113 g/mL, Cedarlane Laboratories, Hornby, Ontario, Canada) according to the manufacturer's instructions.

### 2.3 Fluorescence Labeling of CD34+ Cells and Jurkat Cells for Confocal Analysis

Jurkat and CD34+ cells were suspended ( $0.5 \times 10^6/\text{mL}$ ) in prewarmed ( $37^\circ\text{C}$ ) RPMI medium containing 500 nM Mito Tracker Red (M-7512, Molecular Probes, Invitrogen) and incubated for 30 min in a humidified atmosphere at  $37^\circ\text{C}$  and 5%  $\text{CO}_2$ . After incubation the cells were plated on poly-L-lysine (Sigma, St. Louis, Missouri)-coated cover glass slips. The cells were fixed

with freshly prepared 3.7% paraformaldehyde (Sigma) and permeabilized by incubating in 0.2% Triton X-100 (EMD Chemicals, Gibbstown, New Jersey) for 5 min. The nucleic acid stain SYTOX Green (Molecular Probes) was then added (100 nM). The slide was kept covered in foil until confocal microscopic analysis.

#### 2.4 Finite-Difference Time-Domain Simulation

In the past we applied Mie theory to analyze the 2D light scattering patterns obtained from various sizes of polystyrene beads.<sup>16</sup> These 2D light scattering patterns have a symmetric fringe structure, which is due to the homogeneous spherical property of the beads, as also observed by other groups.<sup>21</sup> Here we study the light scattering from hematopoietic cells. Compared with polystyrene beads, cells have various organelles with different optical properties, resulting in a heterogeneous structure. It is a challenge to apply Mie theory for the exact simulation of light scattering from cells, due to the boundary conditions required to solve the Maxwell's equations. For the study of cells with various organelles, a numerical solution such as the finite-difference time-domain (FDTD) method is usually adopted.<sup>22–28</sup>

We have developed a FDTD code (AETHER) for the simulation of light scattering from irregularly-shaped, heterogeneous cells.<sup>15,25</sup> The AETHER FDTD code solves the Maxwell's equations in a three-dimensional (3D) grid in the near-field of the scatterer. A Liao absorption boundary condition is applied to terminate the 3D calculations.<sup>29</sup> In AETHER, a near- to far-field transformation is performed so that the experimental light scattering patterns which are in the far field can be compared with those from FDTD simulations.

### 3 Results and Discussion

#### 3.1 Comparison of the 2D Experimental Light Scattering Patterns with AETHER Simulations

Recent studies have experimentally demonstrated that the mitochondria are the main contributors for light scattering from cells.<sup>9,15,30</sup> Mitochondria have been implicated in many diseases such as cancer, Alzheimer's, and Parkinson's,<sup>31,32</sup> hence understanding light scattering from mitochondria in single cells is of value in the future treatment of these diseases.<sup>33,34</sup> Mitochondria are organelles of nanometer to micrometer size and may be distributed throughout a cell. Because of the diffraction limit, optical microscopy cannot produce a well resolved image of mitochondria. However, information about mitochondria can be obtained from studying the 2D light scattering patterns from single cells.<sup>15</sup> In this section, a detailed analysis of AETHER simulations is used to determine the various mitochondrial contributions to the 2D light scattering patterns. The experimental 2D light scattering patterns from Jurkat cells and CD34+ cells are then compared with simulations. In the simulations simplified artificial models for optical properties of cells are used. In order to confirm that the choice of these models is reasonable, we performed laser scanning confocal fluorescence imaging of the Jurkat and the CD34+ cells (see Sec. 3.2).

In order to study the mitochondrial contributions to the 2D light scattering patterns, the Jurkat cell is assumed to be spherical with randomly distributed mitochondria, and a nucleus located at the center. The cytoplasm (Fig. 2, magenta, as shown in the

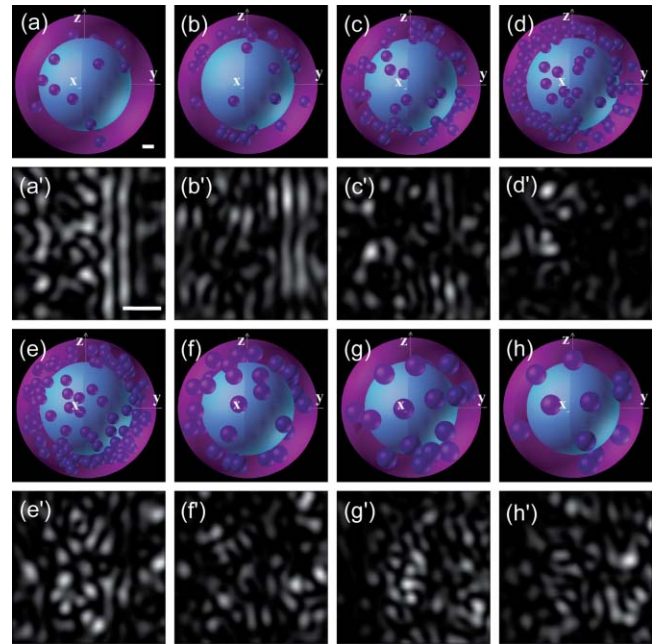


**Fig. 2** Effects of the number and size of mitochondria on the 2D light scattering patterns. (a)–(h) are cell models used for the AETHER simulations and (a')–(h') are the corresponding 2D light scattering patterns. There are 15, 30, 60, 90, and 120 mitochondria of diameter 1  $\mu\text{m}$  in (a)–(e), respectively. In (f), there are 35 mitochondria of diameter 1.5  $\mu\text{m}$ . In (g), there are 20 mitochondria of diameter 1.8  $\mu\text{m}$ . In (h), there are 15 mitochondria of diameter 1.8  $\mu\text{m}$ . (e), (f), and (g) have approximately the same total volume of mitochondria. (d) and (h) have approximately the same total volume of mitochondria. The scale bar for the cell model is 1  $\mu\text{m}$ , and is 500  $\mu\text{m}$  for the 2D light scattering patterns.

cell models) has a refractive index of 1.35 with a cell diameter of 12  $\mu\text{m}$ . The nucleus (cyan) diameter is 8  $\mu\text{m}$ , with a refractive index of 1.39. The refractive index for the mitochondria (blue) is 1.42. The surrounding medium has a refractive index of 1.334. These refractive index values of the cell components are based on recent publications.<sup>9,10,15,23,25,30</sup> For the simulations in this work, an incident wavelength of 532 nm was used. The 2D light scattering patterns are obtained by assuming that the cell models are in a microfluidic channel as shown in Fig. 1. The scattered light from a single cell travels through a layer of water (100  $\mu\text{m}$ , refractive index 1.334), a glass substrate (1.1  $\mu\text{m}$ , 1.47), a layer of air (300  $\mu\text{m}$ , 1.0), the CCD cover glass (0.75  $\mu\text{m}$ , 1.5), and another layer of air (1.25  $\mu\text{m}$ , 1.0) onto a CCD sensor (Silica, refractive index 4.15). The light scattering pattern discussed in this paper has a dimension of about 2.0 mm horizontally, which corresponds to the light scattering in a 30 deg cone angle (from 75 to 105 deg in a polar angle).

The various optical property models for Jurkat cells and their corresponding simulated 2D light scattering patterns are shown in Fig. 2. In Figs. 2(a)–2(e), we increased the mitochondria number from 15, 30, 60, 90, to 120, while keeping the size (1.0  $\mu\text{m}$ ) unchanged. From Fig. 2(a') we notice that the 2D light scattering patterns have both the small-scale 2D structures (blob-like structures) and the fringes. When the number of mitochondria changes to 30, we still obtain similar light scattering patterns [Fig. 2(b')] as in Fig. 2(a'). However, when the number of mitochondria increases to 60 or more in Figs. 2(c'), 2(d'), and 2(e'),

we obtain only small-scale 2D structures. In Figs. 2(e), 2(f), and 2(g), the volume of the mitochondria is fixed but with varying size and number. There are 35 mitochondria with a diameter of  $1.5\ \mu\text{m}$  in Fig. 2(f), and 20 mitochondria of a diameter of  $1.8\ \mu\text{m}$  [Fig. 2(g)]. We observe that they give similar small-scale 2D structure patterns. When we reduce the mitochondria number from 20 [Fig. 2(g)] to 15 [Fig. 2(h)], the 2D light scattering patterns are still dominated by the small-scale 2D structures.

We observe that when the mitochondria volume fraction in a cell is above a certain value, here 3.5% [Fig. 2(d)], the cell light scattering pattern will be dominated by small-scale 2D structures. In typical cells, the mitochondria volume fraction is above 5%, thus it is reasonable to expect small-scale 2D structures to be present in the experimental light scattering patterns providing the mitochondria are main contributors to the 2D light scattering patterns. We understand that real cells have much more complex organelle distributions than what we assumed here in Fig. 2. However, given that the indices of refraction for mitochondria typically have the largest values among the cellular organelles, it is justified to perform simulations with such simplified cell models. We also observed that when the volume fraction of the mitochondria is fixed, the simulated 2D light scattering patterns are insensitive to the number of mitochondria [see Figs. 2(e'), 2(f'), and 2(g')]. No significant change of the light scattering patterns was observed even after the volume fraction is changed by 25% [see Figs. 2(g') and 2(h')]. These observations from the FDTD simulation results will help us to understand the difference between the 2D light scattering patterns from the Jurkat and the CD34+ cells as will be discussed in Sec. 3.3.

The comparisons between the experimental and simulated 2D light scattering patterns from the Jurkat and CD34+ cells are shown in Fig. 3. Figures 3(a) and 3(b) show the representative experimental 2D light scattering pattern from a Jurkat cell and a CD34+ cell, respectively. In Fig. 3(a), the light scattering pattern is dominated by the many small-scale 2D structures. In Fig. 3(b), the size of the 2D structures increases and their number decreases as compared with Fig. 3(a). From our detailed numerical study discussed earlier, we found that the light scattering patterns are insensitive to the change of mitochondria number and volume. The experimental light scattering pattern of a Jurkat cell [Fig. 3(a)] is similar to the simulated light scattering patterns shown in Figs. 2(e)–2(h). However, the experimental light scattering pattern of a CD34+ cell [Fig. 3(b)] is significantly different from those shown in Figs. 2(e)–2(h) in terms of both the number and the sizes of their small-scale 2D structures.

We will show that the differences in light scattering patterns between Jurkat and CD34+ cells can be attributed to their mitochondrial distributions. Figure 3(d) shows a cell model for CD34+ cell. In this model, we assume there are 72 mitochondria with a diameter of  $1\ \mu\text{m}$ , aggregated in an ellipsoid with two long axes of  $8\ \mu\text{m}$  along  $x$  and  $y$ , and a short axis of  $4\ \mu\text{m}$  along  $z$ . The corresponding simulated 2D light scattering pattern is shown in Fig. 3(f). The simulated 2D light scattering pattern reproduced the key features of the experimental 2D light scattering pattern of a CD34+ cell. To further explore the effects of mitochondrial aggregation on the 2D scatter patterns, the aggregated mitochondria in Fig. 3(d) are redistributed randomly as shown in Fig. 4(a). Figure 4(b) shows the corresponding simulated 2D light scattering pattern for randomly distributed

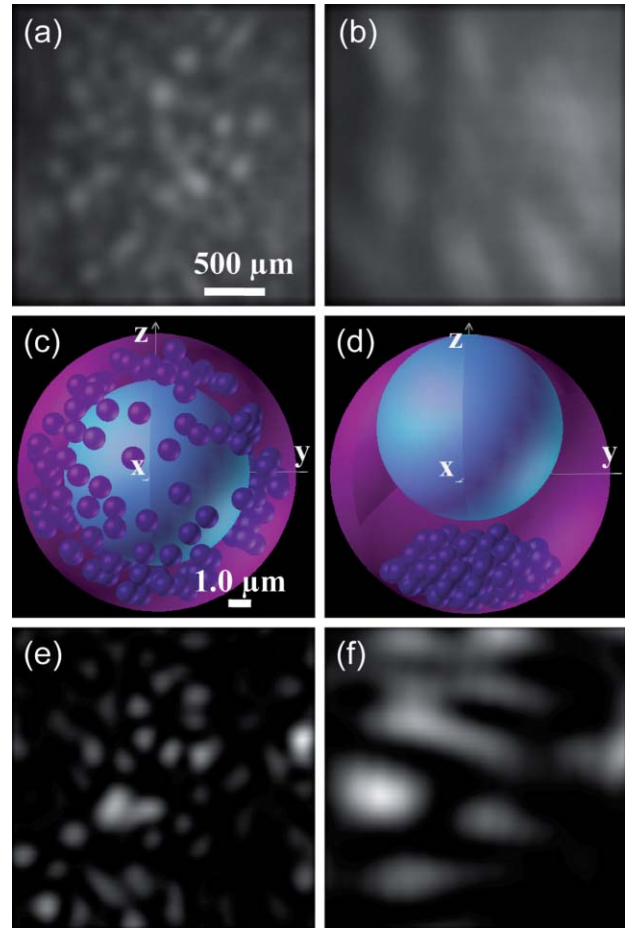


**Fig. 3** Two-dimensional light scattering patterns from Jurkat and CD34+ cells. (a) and (b) are the representative experimental 2D light scattering patterns from a Jurkat cell and a CD34+ cell, respectively. (c) and (d) are the simplified optical properties models for the two cells. The cytoplasm is  $12\ \mu\text{m}$  in diameter and the nucleus is  $8\ \mu\text{m}$  in diameter. In (c), there are 120 mitochondria, each with a diameter of  $1\ \mu\text{m}$ . In (d), there are 72 mitochondria, each with a diameter of  $1\ \mu\text{m}$ . (e) and (f) are the 2D FDTD light scattering patterns for the cell models (c) and (d), respectively.

mitochondrial model of Fig. 4(a). The randomly distributed mitochondria give a pattern similar to those of Jurkat cell light scattering patterns. The above analysis indicates that the difference between the experimental scatter patterns of Fig. 3(a) and 3(b) may be due to how the mitochondria are distributed within the cells as suggested by our numerical study. In particular the numerical simulations suggest that the mitochondria in a Jurkat cell would have a random distribution and an aggregated distribution for a CD34+ cell. In Sec. 3.2, we will show these results are consistent with those obtained from our study using laser scanning confocal fluorescence imaging. In Sec. 3.3, we will further discuss and present the quantitative analysis of experimental and numerical results that have been discussed thus far.

### 3.2 Laser Scanning Confocal Fluorescence Imaging of Cells

In Sec. 3.1, the study of the light scattering patterns from Jurkat and CD34+ cells, we compared the experimental results with

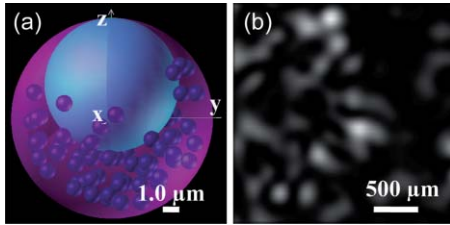


**Fig. 4** (a) An optical properties model with 72 mitochondria of diameter of 1  $\mu\text{m}$ . Note this is the same number of mitochondria as in Fig. 3(d) but in this case the mitochondria are randomly distributed throughout the entire cell, while in Fig. 3(d) the mitochondria are aggregated. (b) is the corresponding simulated 2D light scattering pattern.

those from FDTD simulations. The results suggested that the mitochondrial distribution for a CD34+ cell may be aggregated while that for a Jurkat cell may be random. It is important to verify these results using another independent technique.

Figure 5 shows the laser scanning confocal fluorescence imaging of Jurkat and CD34+ cells. The experiments were performed on a Fluoview300 confocal microscope (Olympus, Germany). The cells were labeled for nucleus and mitochondria and a sequential scanning of the cells was performed. Shown in Fig. 5(a) is the confocal image of the labeled mitochondria in a Jurkat cell, and Fig. 5(b) is the labeled nucleus in the Jurkat cell. Figure 5(c) is the overlay of Figs. 5(a) and 5(b). Similarly, Figs. 5(d), and 5(f) show the results for the CD34+ cell. From the confocal imaging results, we observe that the mitochondria in the Jurkat cell are randomly distributed in the whole cell. However, in the CD34+ cell, there are aggregated mitochondria in the lower part of the cell. The phenomenon of aggregated mitochondria in cells has also been observed by others in the study of cell apoptosis.<sup>35–37</sup>

### 3.3 Analysis of the 2D Light Scattering Patterns

In conventional flow cytometry, the fluorescence signals from the labeled organelles inside cells are used for cell sorting and cell determination. Our results have shown that the light scatter-

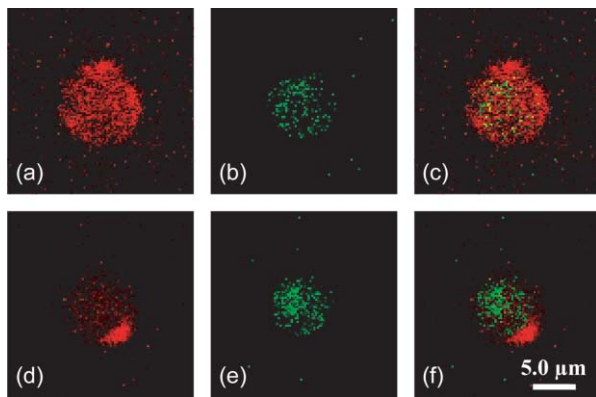


**Fig. 5** Representative confocal fluorescence images of Jurkat and CD34+ cells. (a) and (b) show the mitochondria (red) and the nucleus (green) in a Jurkat cell. Figure (c) is the overlay of (a) and (b). Similarly, (d)–(f) show the results for the CD34+ cell. We observe that the mitochondria are randomly distributed in the Jurkat cell and are aggregated in the CD34+ cell.

ing patterns from different cells are distinctive and that useful parameters may be obtained by analyzing the 2D light scattering patterns. We expect that these parameters or observables may have similar functions as those obtained in commercial flow cytometers, but with the advantage of being label-free. Consequently, we analyzed the 2D light scattering patterns to extract characteristics that may be used for cell discrimination.

We adopt here a speckle analysis of the obtained 2D light scattering patterns. Whenever a coherent light of a laser probe is scattered by randomly distributed centers, the light collected on the 2D screen of a CCD sensor forms an interference pattern that varies randomly in space and is known as speckle (more precisely the maxima, here the small-scale 2D structures, are 2D cross sections of the speckles which are 3D objects). A comparison between the spectra in Figs. 3(e) and 3(f) shows how transition from the randomly distributed mitochondria in Fig. 3(c) to the aggregated distribution of mitochondria in Fig. 3(d) modifies speckle distributions. The random pattern of Fig. 3(e) has evolved toward the interference pattern Fig. 3(f) reminiscent of the scattering on the large structures such as cell cytoplasm or nucleus. Comparisons between Figs. 3(f) and 4(b) demonstrate how the speckle patterns are formed with the increasing randomness of the mitochondria distributions.

The statistical properties of these 2D speckle cross sections will be used in the quantitative analysis of the numerical and experimental pattern of scattered light. We proceed by first counting how many local intensity maxima are in each 2D light scattering pattern and next by calculating their average area. These two observables, i.e., the number of speckles and the average area of their cross sections will be used as parameters for cell determination.

Figure 6 shows the analysis of the 2D light scattering patterns in Figs. 3(a), 3(b), 3(e), and 3(f). For the Jurkat cell experimental

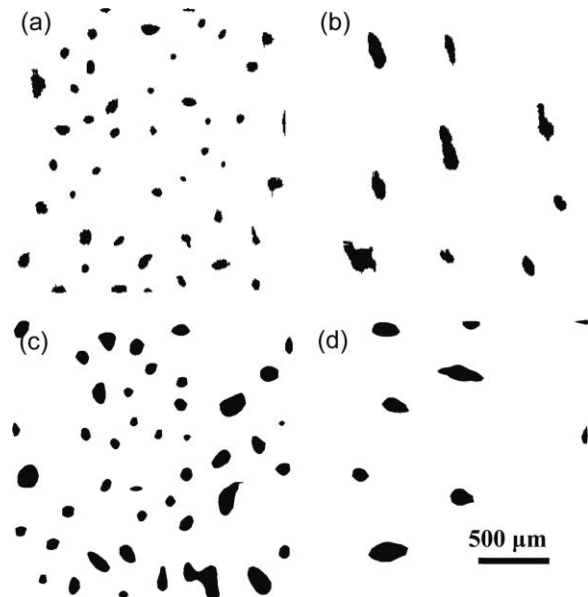


**Fig. 6** Analysis of the experimental and simulation 2D light scattering patterns. The speckle number and their average cross-sectional area are used for the discrimination of cells. (a)–(d) are the pattern analysis results for the 2D light scattering patterns in 3(a), (b), (e), and (f), respectively.

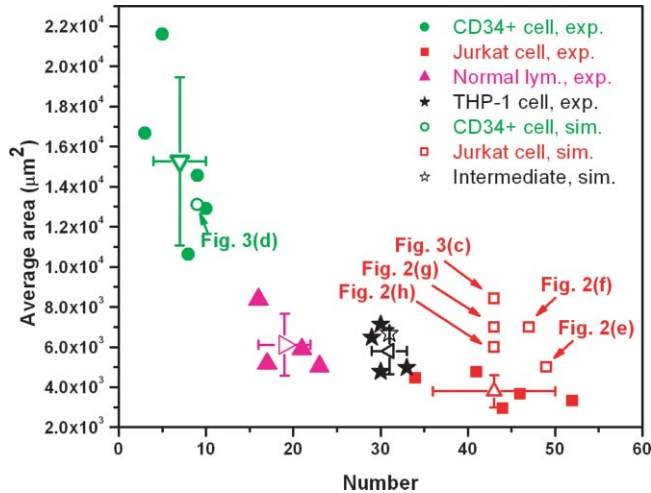


**Fig. 7** Label-free method for discrimination of cells. The small-scale 2D structures in the light scattering patterns are analyzed. Parameters of the average area for all the 2D structures and the total number of these structures in each 2D light scattering pattern are used for the determination of cells. The experimental results agree well with those of the FDTD simulations for both Jurkat cells and CD34+ cells. The FDTD result (intermediate) based on the model of Fig. 4(a), agrees well with the THP-1 experimental results.

light scattering pattern [Fig. 6(a)], there are 46 speckles in total with an average area of  $0.0037 \text{ mm}^2$ . In Fig. 6(b), the CD34+ cell experimental light scattering pattern has 9 local maxima with an average area of  $0.0146 \text{ mm}^2$ . The simulated light scattering patterns using the Jurkat cell model [Fig. 6(c)] produces 43 speckles with an area parameter of  $0.0084 \text{ mm}^2$ , while in the CD34+ cell model there are 9 maxima with an average area of  $0.0131 \text{ mm}^2$ .

The parameters obtained from different cells are plotted in Fig. 7, which reveals that CD34+ cells and Jurkat cells form well separated clusters in the plots, similar to a conventional flow cytometric plot. This is due to the fact that CD34+ cells and Jurkat cells are very different. The AETHER simulation results for the CD34+ and the Jurkat cell models are in reasonable agreement as compared with the experimental results. In this case, the speckle number and the average area for their cross sections in the 2D light scattering patterns may be used for cell determination. Since the CD34+ cells are normal cells, while the Jurkat cells are malignant cells, our results agree with the recent studies showing that in normal cells the mitochondria aggregate, causing apoptosis, while in malignant cells the mitochondria are randomly distributed in the whole cells.<sup>35–37</sup> The method we developed here detects those two mitochondrial distributions in single cells in a label-free manner.

Results obtained from acute monocytic leukemia THP-1 cells and normal lymphocytes are also shown in Fig. 7. We found that the THP-1 cell results form a cluster next to the cluster of the Jurkat cell results, while the cluster of the normal lymphocytes is located in between those of CD34+ cells and the THP-1 cells. The FDTD result for the 72 randomly distributed mitochondria [Fig. 4(a)] correlates well with the THP-1 cell results. Inclusion of these malignant and normal cells illustrates the value of the method developed here for its use in future discrimination between these various cell types.

Here we also show the mean and the standard deviation (SD) for Jurkat cells, THP-1 cells, normal lymphocytes and CD34+ cells as open triangles with different orientations (Fig. 7). The Jurkat cells have  $43 \pm 7$  maxima, with an average area of  $0.0038 \pm 0.0008 \text{ mm}^2$ . The THP-1 cells have  $30 \pm 9$  speckles and the average cross-sectional area is  $0.0047 \pm 0.0008 \text{ mm}^2$ . The speckle number and the average cross-sectional area for the CD34+ cells are  $7 \pm 3$  and  $0.0153 \pm 0.0042 \text{ mm}^2$ , respectively. Parameters for normal lymphocytes are  $19 \pm 3$  and  $0.0061 \pm 0.0016 \text{ mm}^2$ . Thus, generally speaking, the normal cells (CD34+ cell and normal lymphocytes) can be discriminated from leukemic cells (Jurkat and THP-1 cells).

## 4 Summary

We have presented here a label-free technique based on 2D light scattering patterns for the determination of mitochondrial distributions in single cells in a microfluidic platform. The acquisition of 2D light scattering patterns was achieved by employing a microfluidic cytometer in which laser light was fiber-coupled into the microfluidic channel. Experimental 2D light scattering patterns from different cells were compared with those obtained from the simulations using our AETHER FDTD code. The results suggested the different experimental light scattering patterns obtained for Jurkat and CD34+ cells may be due to the fact that the mitochondria are randomly distributed in Jurkat cells, while they are aggregated in CD34+ cells. The cell models used in the simulations are good mimics as confirmed by the confocal fluorescence cell images. The label-free technique we developed here for cell determination is based on two observables, namely the number of the speckles and their average cross-sectional area in a 2D light scattering pattern. We showed that this method may be used for the discrimination between normal hematopoietic cells (CD34+ cells and lymphocytes) and leukemic cells (Jurkat and THP-1 cells). With further development, this technique has the potential for use in the physiological monitoring of human blood cells in clinics for detection of hematologic malignancy.

## Acknowledgments

The authors acknowledge the financial support of Canadian Institute for Photonic Innovations, MicroSystems Technology Research Initiative of University of Alberta, and Natural Sciences and Engineering Research Council of Canada, and Canadian Blood Services/Canadian Institute of Health Research. We thank WestGrid of the University of Alberta for parallel computation support; NanoFab of University of Alberta for the support of microchip fabrication; the Integrated Nanosystems Research Facility of the University of Alberta for providing the confocal microscopy facility; and Alois Harmony from Department of Medicine for useful discussion about confocal microscopy.

## References

1. T. Horio and H. Hotani, "Visualization of the dynamic instability of individual microtubules by dark-field microscopy," *Nature (London)* **321**(6070), 605–607 (1986).
2. A. Hernandezcruz, F. Sala, and P. R. Adams, "Subcellular calcium transients visualized by confocal microscopy in a voltage-clamped vertebrate neuron," *Science* **247**(4944), 858–862 (1990).

3. B. Huang, S. A. Jones, B. Brandenburg, and X. W. Zhuang, "Whole-cell 3D STORM reveals interactions between cellular structures with nanometer-scale resolution," *Nat. Methods* **5**(12), 1047–1052 (2008).
4. D. B. Williams and C. B. Carter, *Transmission Electron Microscopy: A Textbook for Materials Science*, Plenum Press, New York (1996).
5. A. Janowska-Wieczorek, M. Majka, J. Ratajczak, and M. Z. Ratajczak, "Autocrine/paracrine mechanisms in human hematopoiesis," *Stem Cells* **19**(2), 99–107 (2001).
6. E. A. Copelan, "Medical progress: Hematopoietic stem-cell transplantation," *N. Engl. J. Med.* **354**(17), 1813–1826 (2006).
7. L. A. Marquez-Curtis, A. R. Turner, L. M. Larratt, B. Letcher, S. F. Lee, and A. Janowska-Wieczorek, "CD34+ cell responsiveness to stromal cell-derived factor-1 alpha underlies rate of engraftment after peripheral blood stem cell transplantation," *Transfusion* **49**(1), 161–169 (2009).
8. G. C. Salzman, M. E. Wilder, and J. H. Jett, "Light-scattering with stream-in-air flow systems," *J. Histochem. Cytochem.* **27**(1), 264–267 (1979).
9. J. R. Mourant, J. P. Freyer, A. H. Hielscher, A. A. Eick, D. Shen, and T. M. Johnson, "Mechanisms of light scattering from biological cells relevant to noninvasive optical-tissue diagnostics," *Appl. Optics* **37**(16), 3586–3593 (1998).
10. R. Drezek, A. Dunn, and R. Richards-Kortum, "Light scattering from cells: finite-difference time-domain simulations and goniometric measurements," *Appl. Optics* **38**(16), 3651–3661 (1999).
11. V. Backman, V. Gopal, M. Kalashnikov, K. Badizadegan, R. Gurjar, A. Wax, I. Georgakoudi, M. Mueller, C. W. Boone, R. R. Dasari, and M. S. Feld, "Measuring cellular structure at submicrometer scale with light scattering spectroscopy," *IEEE J. Sel. Top. Quantum Electron.* **7**(6), 887–893 (2001).
12. G. Schuele, E. Vitkin, P. Huie, C. O'Connell-Rodwell, D. Palanker, and L. T. Perelman, "Optical spectroscopy noninvasively monitors response of organelles to cellular stress," *J. Biomed. Opt.* **10**(5), 051404 (2005).
13. H. Fang, L. Qiu, E. Vitkin, M. M. Zaman, C. Andersson, S. Salahuddin, L. M. Kimerer, P. B. Cipolloni, M. D. Modell, B. S. Turner, S. E. Keates, I. Bigio, I. Itzkan, S. D. Freedman, R. Bansil, E. B. Hanlon, and L. T. Perelman, "Confocal light absorption and scattering spectroscopic microscopy," *Appl. Optics* **46**(10), 1760–1769 (2007).
14. I. Itzkan, L. Qiu, H. Fang, M. M. Zaman, E. Vitkin, L. C. Ghiran, S. Salahuddin, M. Modell, C. Andersson, L. M. Kimerer, P. B. Cipolloni, K. H. Lim, S. D. Freedman, I. Bigio, B. P. Sachs, E. B. Hanlon, and L. T. Perelman, "Confocal light absorption and scattering spectroscopic microscopy monitors organelles in live cells with no exogenous labels," *Proc. Natl. Acad. Sci. U.S.A.* **104**(44), 17255–17260 (2007).
15. X. T. Su, C. Capjack, W. Rozmus, and C. Backhouse, "2D light scattering patterns of mitochondria in single cells," *Opt. Express* **15**(17), 10562–10575 (2007).
16. X. T. Su, K. Singh, C. Capjack, J. Petracek, C. Backhouse, and W. Rozmus, "Measurements of light scattering in an integrated microfluidic waveguide cytometer," *J. Biomed. Opt.* **13**(2), 024024 (2008).
17. H. Subramanian, P. Pradhan, Y. Liu, I. R. Capoglu, X. Li, J. D. Rogers, A. Heifetz, D. Kunte, H. K. Roy, A. Taflove, and V. Backman, "Optical methodology for detecting histologically unapparent nanoscale consequences of genetic alterations in biological cells," *Proc. Natl. Acad. Sci. U.S.A.* **105**(51), 20118–20123 (2008).
18. X. T. Su, S. E. Kirkwood, M. Gupta, L. Marquez-Curtis, Y. Y. Qiu, A. Janowska-Wieczorek, W. Rozmus, and Y. Y. Tsui, "Microscope-based label-free microfluidic cytometry," *Opt. Express* **19**(1), 387–398 (2011).
19. Z. Wang, J. El-Ali, M. Engelund, T. Gotsaed, I. R. Perch-Nielsen, K. B. Mogensen, D. Snakenborg, J. P. Kutter, and A. Wolff, "Measurements of scattered light on a microchip flow cytometer with integrated polymer based optical elements," *Lab Chip* **4**(4), 372–377 (2004).
20. A. Janowska-Wieczorek, L. A. Marquez, J. M. Nabholz, M. L. Cabuhat, J. Montano, H. Chang, J. Rozmus, J. A. Russell, D. R. Edwards, and A. R. Turner, "Growth factors and cytokines upregulate gelatinase expression in bone marrow CD34(+) cells and their transmigration through reconstituted basement membrane," *Blood* **93**(10), 3379–3390 (1999).
21. K. M. Jacobs, J. Q. Lu, and X. H. Hu, "Development of a diffraction imaging flow cytometer," *Opt. Lett.* **34** (19), 2985–2987 (2009).
22. A. Taflove, *Computational Electrodynamics: The Finite-Difference Time-Domain Method*, Artech House, Norwood, MA (1995).
23. A. Dunn and R. Richards-Kortum, "Three-dimensional computation of light scattering from cells," *IEEE J. Sel. Top. Quantum Electron.* **2**(4), 898–905 (1996).
24. X. Li, A. Taflove, and V. Backman, "Recent progress in exact and reduced-order modeling of light-scattering properties of complex structures," *IEEE J. Sel. Top. Quantum Electron.* **11**(4), 759–765 (2005).
25. C. G. Liu, C. Capjack, and W. Rozmus, "3-D simulation of light scattering from biological cells and cell differentiation," *J. Biomed. Opt.* **10**(1), 014007 (2005).
26. J. Q. Lu, P. Yang, and X. H. Hu, "Simulations of light scattering from a biconcave red blood cell using the finite-difference time-domain method," *J. Biomed. Opt.* **10**(2), 024022 (2005).
27. M. S. Starosta and A. K. Dunn, "Three-Dimensional Computation of Focused Beam Propagation through Multiple Biological Cells," *Opt. Express* **17**(15), 12455–12469 (2009).
28. G. S. Chao and K. B. Sung, "Investigating the spectral characteristics of backscattering from heterogeneous spherical nuclei using broadband finite-difference time-domain simulations," *J. Biomed. Opt.* **15**(1), 015007 (2010).
29. Z. P. Liao, H. L. Wong, B. Yang, and Y. Yuan, "A Transmitting Boundary for Transient Wave Analyses," *Sci. Sinica Ser. A* **27**(10), 1063–1076 (1984).
30. J. D. Wilson, C. E. Bigelow, D. J. Calkins, and T. H. Foster, "Light scattering from intact cells reports oxidative-stress-induced mitochondrial swelling," *Biophys. J.* **88**(4), 2929–2938 (2005).
31. S. Desagher and J. C. Martinou, "Mitochondria as the central control point of apoptosis," *Trends Cell Biol.* **10**(9), 369–377 (2000).
32. P. A. Trimmer, R. H. Swerdlow, J. K. Parks, P. Keeney, J. P. Bennett, S. W. Miller, R. E. Davis, and W. D. Parker, "Abnormal mitochondrial morphology in sporadic Parkinson's and Alzheimer's disease cybrid cell lines," *Exp. Neurol.* **162**(1), 37v50 (2000).
33. C. S. Mulvey, A. L. Curtis, S. K. Singh, and I. J. Bigio, "Elastic scattering spectroscopy as a diagnostic tool for apoptosis in cell cultures," *IEEE J. Sel. Top. Quantum Electron.* **13**(6), 1663–1670 (2007).
34. X. T. Su, K. Singh, W. Rozmus, C. Backhouse, and C. Capjack, "Light scattering characterization of mitochondrial aggregation in single cells," *Opt. Express* **17**(16), 13381–13388 (2009).
35. N. Haga, N. Fujita, and T. Tsuruo, "Involvement of mitochondrial aggregation in arsenic trioxide (As<sub>2</sub>O<sub>3</sub>)-induced apoptosis in human glioblastoma cells," *Cancer Sci.* **96**(11), 825–833 (2005).
36. W. D. Thomas, X. D. Zhang, A. V. Franco, T. Nguyen, and P. Hersey, "TNF-related apoptosis-inducing ligand-induced apoptosis of melanoma is associated with changes in mitochondrial membrane potential and perinuclear clustering of mitochondria," *J. Immunol.* **165**(10), 5612–5620 (2000).
37. L. Y. Liu, A. Vo, G. Q. Liu, and W. L. McKeehan, "Distinct structural domains within C19ORF5 support association with stabilized microtubules and mitochondrial aggregation and genome destruction," *Cancer Res.* **65**(10), 4191–4201 (2005).